American Mineralogist, Volume 78, pages 477–485, 1993

X-ray absorption spectroscopy of Fe, Mn, Zn, and Ti structural environments in staurolite

C.M.B. Henderson, J. M. Charnock
Department of Geology, The University, Manchester M13 9PL, U.K.
J. V. Smith
Department of Geophysical Sciences and Consortium for Advanced Radiation Sources, University of Chicago, Chicago, Illinois 60637, U.S.A.
G. N. Greaves
SERC Laboratory, Daresbury, Warrington WA4 4AD, U.K.

Abstract

The local site geometries of Fe, Mn, Zn, and Ti in staurolite from Pizzo Forno, Switzerland, have been determined by X-ray absorption spectroscopy (XAS) and the results used to deduce the crystallographic sites occupied by these elements. For each element, structural assignments are based on the positions and intensities of preedge, edge, and near-edge features, as well as on refined extended X-ray absorption fine structure (EXAFS) data.

The least-squares refined, mean first-shell metal-O bond length, coordination number, and Debye-Waller factor for Fe (10.24 wt%) are 1.99 Å, 3.6, and 0.016 Å^2, for Mn (0.14 wt%) they are 2.01 Å, 4.0, and 0.012 Å^2, and for Zn (0.21 wt%) they are 1.95 Å, 5.1, and 0.018 Å^2, respectively. These values, together with preedge and near-edge data, suggest that Fe and Mn are predominantly present as divalent cations in the tetrahedrally coordinated T2 site. At least 70% of the Zn is also in the T2 site, but $^{[6]}$Zn could also be present. Ti preedge and edge features and refined first-shell EXAFS are consistent with Ti (0.40 wt%) being present as Ti^{4+} in distorted octahedral coordination, most likely in the M2 site.

Minor concentrations of Mn (1400 ppm) and Zn (2100 ppm) can provide reliable EXAFS site geometry information out to 5 Å (i.e., as far as for major Fe), which demonstrates the utility of the element-specific XAS technique in elucidating the structures of chemically complex minerals such as staurolite.

Introduction

Although the general structural relations of staurolite are fairly well established (Náray-Szabó and Sasvári, 1958; Smith, 1968; Hawthorne et al., 1993) and the probable location of protons determined (Takéuchi et al., 1972; Ståhl et al., 1988), important crystal chemical problems remain to be resolved (Holdaway et al., 1986, 1991). Much contradictory information has been published regarding the distribution of Fe^{2+} among different crystallographic sites, although detailed Mössbauer studies for a large sample set have recently resolved many of these problems (Dyar et al., 1991). Differing approaches have been used to assign the ubiquitous, but less abundant, divalent cations Zn, Mg, Mn, and Co to particular sites. The environment of Ti is also uncertain. The usefulness of staurolite in aiding the modeling of *P-T* conditions for formation of metamorphic assemblages depends on the adoption of reliable stoichiometric formulae (e.g., Yardley, 1981; Holdaway et al., 1986, 1991) so that end-member mineral component activities can be appropriately defined. It is also necessary to obtain a clear understanding of the site occupancies of minor elements, as Zn (e.g., Guidotti, 1970; Ashworth, 1975) and Li (Dutrow et al., 1986) are believed to extend the upper temperature stability of staurolite, whereas Mn reduces staurolite stability when in the presence of garnet (Ganguly, 1968).

Direct structural evidence on the environment of the minor cations is difficult to obtain because of their relatively low concentrations and the similarities of their X-ray scattering properties (e.g., Mg and Al, Fe and Mn). Staurolite is not amenable to NMR study because of its high Fe content. Thus we have used the element-specific XAS technique to study directly the local structural environments of Mn, Zn, and Ti. The Fe environment has also been studied to complement the results obtained from X-ray diffraction and Mössbauer spectroscopic methods.

XAS provides spectra consisting of several regions (see the review of Brown et al., 1988). Although structural information is element specific, where an element occurs in several sites an average environment is obtained. Thus

0003–004X/93/0506–0477$02.00

data reduction of EXAFS spectra gives one-dimensional, radial information in the form of average bond lengths, coordination numbers, and Debye-Waller factors (disorder parameters). Preedge, edge, and XANES spectra provide information on valency, coordination number, and site symmetry. Preedge and edge features are often associated with electron transitions to localized states, whereas XANES features result from multiple scattering effects. Overall, edge features provide qualitative, three-dimensional structural information, which is especially rich for transition elements (e.g., Waychunas et al., 1983; Calas and Petiau, 1983; Binsted et al., 1986; Waychunas, 1987). Waychunas et al. (1983) pointed out that more regular structural sites produce sharper features in the edge spectra.

In this work, the results of Fe, Mn, Zn, and Ti K-edge XAS studies are integrated with other data to provide information on the complex crystal chemical relations exhibited by staurolite.

Staurolite crystal chemistry

The crystal structure of staurolite can be considered to consist of layers of essentially kyanite structure parallel to the (010) plane alternating with spinel-like monolayers (Ribbe, 1982). Smith (1968) refined the structure on the basis of seven octahedral and two tetrahedral cation sites. Hawthorne et al. (1993) have recently refined the crystal structures of 42 natural staurolite samples from 17 rocks using the nine cation sites but have revised the original site nomenclature. Thus, the structure consists of one tetrahedral site (T1) and three octahedral sites (M1A, M1B, and M2), all essentially fully occupied, in the kyanite layer, and one tetrahedral site (T2) and four octahedral sites (MA3, M3B, M4A, and M4B), with variable occupancies, in the monolayer. Hawthorne et al. (1993) gave an idealized formula of Fe_{3-4}(T2, M4) $Al_2\square_2$(M3) Al_{16}(M1, M2) Si_8(T1) O_{48} H_{2-4} (sites occupied in parentheses).

Hawthorne et al. (1993) pointed out that staurolite with high H tends to have high occupancies of M4 and low occupancies of M3; in addition, the proximities of T2 and M4 show that they cannot be occupied simultaneously. Ståhl et al. (1988) proposed a structural model containing six types of coexisting domains, the populations of which are believed to depend on which proton sites are occupied, leading in turn to different occupancies of the T2, M3, and M4 sites.

In addition to the elements given in the above formula, minor amounts of Ti, Mn, and Li are ubiquitous, whereas Mg, Zn, Cr, and Co are occasionally enriched to percent concentration levels (see, e.g., Ward, 1984; Dutrow et al., 1986; Bringhurst and Griffin, 1986; Hawthorne et al., 1993). This chemical complexity and the presence of several unfilled structural sites have led to many different assignments of cations. Recent assignments are summarized in Table 1; these models are based mainly on crystal structure determinations, Mössbauer spectroscopy, and crystal chemical considerations.

Previously, the distribution of Fe has been primarily based on the results of Mössbauer studies, with similar spectra being fitted with two, three, four, or five Fe doublets by different workers. In the most comprehensive study, Dyar et al. (1991) presented new data on 23 natural and 12 synthetic staurolite samples. They assigned three separate doublets to Fe^{2+} (averaging 82% of Fe_{tot}) in disordered T2 sites, a doublet to Fe^{2+} in M3 or M4 sites (averaging 11% of Fe_{tot}), a doublet to Fe^{3+} in the T1 site (averaging 5% Fe_{tot} in natural and 8% in synthetic samples), and a possible charge transfer doublet in some samples. Hawthorne et al. (1993) deduced that 76–95% of Fe_{tot} was in $^{[4]}$T2 with the remainder in octahedral sites in decreasing concentration M4 > M2 > M1 > M3. Holdaway et al. (1991) combined the work of Dyar et al. (1991) and the preliminary results of Hawthorne et al. to give the Fe assignments given in Table 1; note that they preferred to assign Fe^{3+} to T2.

Ståhl et al. (1988) and Holdaway et al. (1991) assigned Mn to T2, although other authors prefer the largest octahedral sites (i.e., the M4 sites) (Table 1). Most authors assign Zn to the T2 site, but Ståhl et al. (1988) and Holdaway et al. (1991) also allocated some Zn to the M4 site (Table 1). With the exception of Ståhl et al. (1988), most authors place Ti in the fourfold T2 site (Table 1). Hawthorne et al. (1993) distributed Mn and Ti (also Co and Cr) over M1–M4 and T2 in the same way as for Fe (Table 1).

Smith (1968) concluded that the cation assignment "problem is incapable of a unique solution" and that "staurolite remains an enigma." Taking into account the full range of studies over the last 20 yr it seems that unresolved problems still remain, some of which are amenable to study by the element-specific XAS technique.

Methods and material

The staurolite sample studied is from Pizzo Forno, Switzerland, and was kindly provided by M.J. Holdaway (sample PF2 from Holdaway et al., 1986). The powder used for XAS contained a trace of chlorite as the only impurity. The staurolite sample was finely ground and mounted using Sellotape on Al sample holders. Model compounds were diluted with boron nitride to give an edge step of between 0.5 and 1.5. All spectra were recorded at room temperature. Fe, Mn, and Zn K-edge absorption spectra were obtained on station 7.1 at the Daresbury synchrotron radiation source (SRS) using the transmission mode for all elements in the model compounds and for Fe in staurolite. Fluorescence methods were used for Mn and Zn in staurolite, with the sample at 45° and a single NaI scintillation detector at 90° to the incident beam. Signal to noise ratios were optimized for Mn (and Zn) by placing Cr (Cu) foils (5 or 10 μm thick) in front of the detector to reduce the background. Three to five fluorescence scans were taken and averaged to improve further the signal to noise ratio. K-edge spectra for Ti were obtained on station 8.1 at the SRS with fluorescent radiation detected using a Canberra 13-element energy-dispersive detector. On both beam lines, a Si (111) double-crystal monochromator was used with the crystal

TABLE 1. Published cation site assignments in staurolite

	$^{[4]}$T	$^{[6]}$M1, $^{[6]}$M2	$^{[6]}$M3	$^{[6]}$M4	$^{[4]}$T2	% of Fe_{tot} in $^{[4]}$T2 site	Total occupancy of $^{[4]}$T2 site
Tagai and Joswig (1985)	Si, Fe	Al, Mg	Al, Mg	Fe, Mn	Fe, Al, Ti, Zn	83	76
Holdaway et al. (1986)	Si, Al		Al, Fe^{3+}	Fe, Mn	Fe, Mg, Zn, Li, (Ti)		93
Bringhurst and Griffen (1986)	Si, Al	Al, Mg	Al, Mg, Fe	Fe, Mn	Fe, Al, Co, Ti, Zn	80	95
Ståhl et al. (1988)	Si, Al	Al, Fe^{3+} Mg, Ti, V, Cr	Al, Mg, Ti	Mg, Zn	Fe^{2+}, Li, Mn, Zn, Co	98	75
Alexander (1989)	Si, Fe^{3+}	Al	Al, Fe^{3+}	Fe^{2+}, Mn	Fe^{2+}, Al, Mg, Ti, Zn	92	97
Dyar et al. (1991)	Si, Al, Fe^{3+}		Fe^{2+}		Fe^{2+}, Mg, Li	80	
Holdaway et al. (1991)	Si, Al	Al, Mg, Fe^{2+}	Al, Mg, Fe^{2+}	Fe^{2+}, Zn, Li	Fe^{2+}, Mg, Zn, Li, Ti, Mn, Al, Fe^{3+}	82	92
Hawthorne et al. (1993)	Si, Al	Al, Mg, Fe*	Al, Mg, Fe*	Fe*	Fe*, Zn, Mg, Li, Al	76–95	79–100
Henderson et al. (this work)		Ti (M2)		Zn?	Fe^{2+}, Mn, Zn	>85	

* Includes Fe^{2+}, Fe^{3+}, Mn, Co, Cr, Ti.

faces offset to give 50% rejection of the beam in order to reduce harmonic contamination. The energy scales were calibrated relative to the first inflection points for Fe, Mn, Zn, and Ti metal and have absolute accuracies of about ±1 eV; the precision is better than 1 eV.

Data analysis utilized the single scattering, spherical wave method for calculating EXAFS (Lee and Pendry, 1975), with phase shifts derived from ab initio calculations, using the Daresbury library program EXCURV88 (Binsted et al., 1988), which incorporates the single scattering rapid curved wave theory of Gurman et al. (1984). The phase shift calculations were made using the relaxed 1s core-hole approximation for the central atom, and the program default parameters for the muffin-tin radii, ionic charge, and exchange terms.

No Fourier filtering was used. Spectral fits for the model compounds and for Fe, Mn, and Zn in staurolite were produced by generating theoretical spectra from structures of several shells of backscatterers radially disposed around the central atom, and by allowing parameters defining bond lengths, coordination numbers (first shell only because of overlap between shells of different atoms farther away), and Debye-Waller factors in each shell to vary iteratively to give the best agreement with the experimental spectrum (in R space). E_0 was included as an adjustable parameter in the final fit. Initially, only the first shell was included in the simulation, and the outer shells were added individually, iterating the absorber-scatterer distances and the Debye-Waller factors at each stage. Statistical tests (Joyner et al., 1987) were used to determine whether addition of the shell made a significant improvement to the fit, and only those that were significant at the 1% level were included in the final fit. Relative errors in the first-shell bond distance are ±0.01 Å with probable absolute errors of ±0.02 Å; outer shell distance errors are somewhat larger. Errors for estimated coordination numbers and Debye-Waller factors are about ±20%.

RESULTS AND STRUCTURAL ASSIGNMENTS

Expanded absorption edge regions for Fe, Mn, and Zn in staurolite are displayed in Figure 1, and refined multishell EXAFS data are given in Table 2. For modeling the Fe spectrum, the atom type and coordination numbers chosen for the outer shells were based on those of the T2 site for the structural data of Smith (1968) but do not include O atoms beyond 4 Å, as scattering from these makes an insignificant contribution to the total EXAFS. To test this model, attempts were also made to simulate the EXAFS using atom shells appropriate for the M1–M4 octahedral sites, none of which gave good fits to the experimental spectrum, confirming that most of the Fe is in the tetrahedral T2 site. The Mn and Zn were modeled in the same way. The Mn spectrum gave a very significantly better fit for the T2 site than any of the other sites, whereas for Zn the T2 site gave the best fit, although reasonable fits were also obtained with the octahedral sites. The qualities of the staurolite EXAFS refinement of the models based on the T2 site can be assessed from Figure 2, where experimental and calculated weighted and background-subtracted spectra and the equivalent Fourier transforms are displayed. The EXAFS spectra show interference between scattering from more than one shell of atoms around the central atom, each of which contributes a damped sine wave to the total signal. The Fourier transform of the EXAFS is approximately a radial distribution pair correlation function, and for each metal shows three main groups of backscatterers. Based on X-ray structural information, the first peak is due to the four O atoms in the primary coordination sphere, the second to scattering from 12 Al (M1–M3) atoms at ~3.3 Å, with some contribution from two Fe (T2), two Si (T1), and 12 O atoms, and the third major peak is due to ten Al and four Si atoms at 5.1–5.4 Å (Smith, 1968). Because Al and Si cannot be distinguished because of their similar scattering factors and to account for the range in radial distances from Fe to the 12 Al in the second shell (3.28–3.43 Å), the 12 Al and two Si shells were fitted using two shells of eight and six Al atoms (cf. Table 2). For Fe the multishell EXAFS fit shows excellent agreement (Table 2), with the radial data calculated for the shells associated with the T2 site (Smith, 1968), although the distance at 3.7 Å is rather long. This discrepancy may be due to the absence from the model of contributions from O above 4 Å.

TABLE 2. Radial information from Fe, Mn, and Zn EXAFS spectra for staurolite (PF2)

	EXAFS			
	Shell	N	R (Å)	$2\sigma^2$ (Å^2)
Fe	O	3.6*	1.99	0.015
	O	6	2.93	0.059
	Fe	2	3.35	0.001
	O	6	3.26	0.015
	Al	8	3.36	0.004
	Al	6	3.70	0.023
	Al	10	5.14	0.045
	Si	4	5.53	0.052
Mn	O	4.0*	2.01	0.012
	O	6	3.03	0.053
	Fe	2	3.29	0.001
	O	6	3.33	0.017
	Al	8	3.33	0.002
	Al	6	3.66	0.042
	Al	10	5.12	0.035
	Si	4	5.31	0.035
Zn	O	5.1*	1.96	0.016
	O	6	2.98	0.035
	Fe	2	3.28	0.001
	O	6	3.21	0.016
	Al	8	3.31	0.003
	Al	6	3.67	0.037
	Al	10	5.13	0.033
	Si	4	5.38	0.043

	X-ray**	
Shell	R (Å) range	R (Å) average
4 × O	1.971–2.047	2.008
6 × O	3.179–3.184	3.182
2 × Fe	3.276–3.311	3.294
6 × O	3.328–3.419	3.336
8 × Al	3.277–3.404	3.337
4 × Al + 2 × Si	3.422–3.430	3.427
10 × Al	4.981–5.257	5.166
4 × Si	5.422–5.438	5.430

* Refined first-shell coordination number, others unrefined.
** Radial data calculated for Fe in T2 from X-ray crystal structure (Smith, 1968).

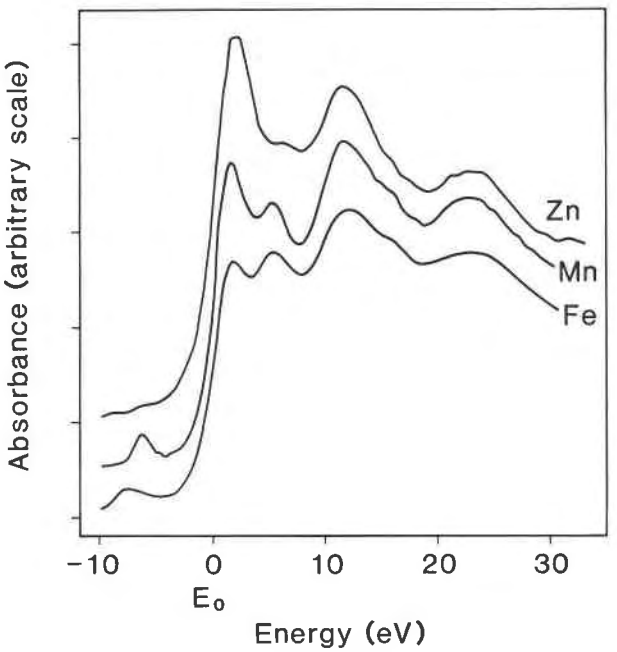

Fig. 1. Background-subtracted K-edge XAS spectra of Fe, Mn, and Zn in staurolite. The spectra for the three elements are aligned relative to their absorption edge values (E_0); note the similarities of the positions of the different features for the three spectra. The absorbance scale is in arbitrary units.

Table 3 includes first metal-O shell data [bond length (R), coordination number (N), and Debye-Waller factor ($2\sigma^2$)], edge position (relative to metallic Fe and Mn), and preedge size (relative to height of the absorption edge) for Fe^{2+}, Fe^{3+}, Mn, and Zn model compounds and staurolite.

Fe

The Fe XANES spectrum shows four well-defined features (Fig. 1) and is identical to those shown for staurolite by Calas and Petiau (1983) and Waychunas et al. (1983). These authors suggested likely electronic transitions responsible for these features. The preedge feature near 7110 eV [−8 eV relative to the absorption edge (E_0) in Fig. 1] results from 1s to 3d transitions and has a significant intensity because of 3d-2p orbital mixing (Calas and Petiau, 1982). In fact, the preedge in staurolite is split, indicating electronic transitions to the 3d t_{2g} and e_g crystal-field energy levels (Calas and Petiau, 1983). The intensity of such preedge features should increase in the order regular octahedral (centrosymmetric), distorted octahedral, and then tetrahedral coordination (noncentrosymmetric). The relative sizes of the preedge peaks thus give a useful indication of site geometry. The other features are at ~7119 (1s-4p), ~7123 ("3rd feature" of Waychunas et al., 1983), and ~7129 eV ("edge crest").

Different types of information can be used to deduce the average environment for the Fe in staurolite. The edge position at 7120 eV (0 eV relative to E_0, Fig. 1) confirms that Fe^{2+} is the dominant oxidation state, with Fe^{3+} being too low in concentration to be detected by K-edge XAS. On the basis of the data of Waychunas et al. (1983) and our own results for various model compounds (cf. Table 3), it seems that Fe^{2+} has preedge intensities in the range 0.055–0.07 for tetrahedral and 0.008–0.025 for octahedral coordination. By contrast, those for Fe^{3+} are in the range 0.10–0.15 for tetrahedral and 0.01–0.025 for octahedral coordination. Thus the size of the preedge peak in staurolite (0.075) is consistent with Fe^{2+} occurring mainly in tetrahedral coordination. On the basis of values for the model compounds, it is clear that the refined first-shell distance and coordination number (Table 3) for staurolite indicate that $^{[4]}Fe^{2+}$ is dominant. Model compound Debye-Waller factors (Table 3) for tetrahedral coordination are smaller than for octahedral coordination, resulting from the decreased static disorder around the metal sites in the former. The Debye-Waller factor for Fe in staurolite is consistent with occupancy of the distorted $^{[4]}$T2 site, although it is significantly larger than for Fe in the framework rubidium iron leucite model

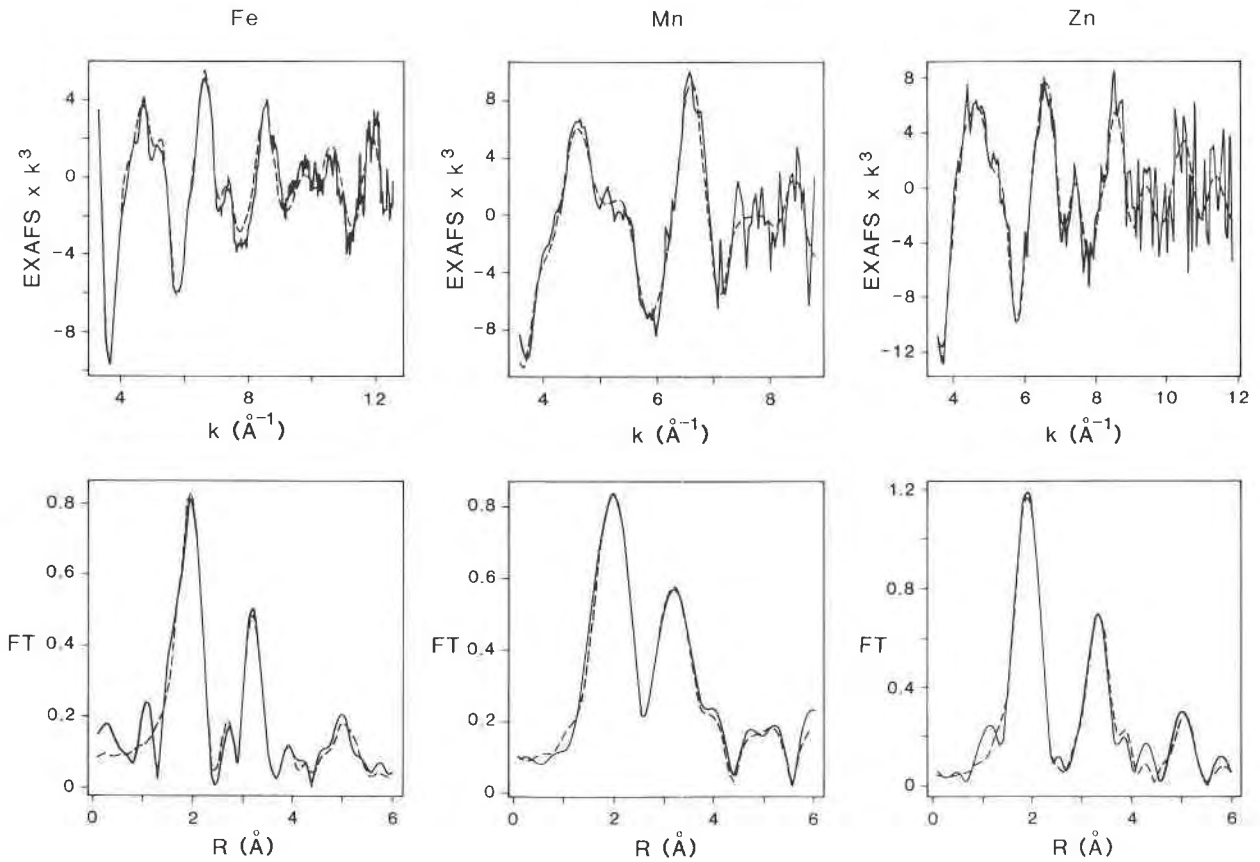

Fig. 2. The k^3-weighted EXAFS (Å^{-3}) and Fourier transforms (FT) corrected for phase shifts for Fe (**left**), Mn (**center**), and Zn (**right**) in Pizzo-Forno (PF2) staurolite. The solid lines represent experimental data and dashed lines the calculated fits to the parameters given in Table 2.

compound. This is consistent with the presence of positional disorder associated with the T2 site in staurolite (Smith, 1968; Alexander, 1989; Ståhl and Legros, 1991; Dyar et al., 1991; Hawthorne et al., 1993). The presence of Fe in octahedral sites would also increase the Debye-Waller factor derived from the observed spectrum, which is an average of all the Fe in the sample. Overall, the average Fe environment deduced from the XAS spectrum is consistent with the dominant Fe species being $^{[4]}Fe^{2+}$ in the T2 site, in agreement with X-ray structure and Mössbauer results. Although it is not possible to be categorical, it seems likely that Fe in other sites makes up $<15\%$ of Fe_{tot} (cf. Table 1).

Mn and Zn

The expanded edge regions for Mn and Zn (Fig. 1) show striking similarities to that for Fe. The positions of the four main features, relative to E_0, coincide within 1 eV, suggesting that Mn, Zn, and Fe have very similar structural environments. For Mn, the 1s-3d preedge (~6356 eV; −7 eV relative to E_0) and 1s-4p (~6544 eV) features are sharper and more intense than for Fe. These differences could reflect either the different electronic structures of the two elements or a more regular tetrahedral coordination polyhedron for Mn. The sharper definition of the edge crest peak for Mn at 6554 eV (12 eV relative to E_0), caused by multiple scattering effects rather than localized electron transitions is consistent with the latter explanation. As Zn^{2+} has a $3d^{10}$ configuration, there is no detectable 1s-3d preedge peak. The 1s-4p feature for Zn (9655 eV; 2 eV relative to E_0) is the most intense feature on the edge structure, and this fact, together with the third edge feature (9665 eV) being narrow and symmetrical (Fig. 1), suggests that Zn has the most regular T2 site environment.

The refined EXAFS for Mn (Fig. 2) show Fourier transform peak widths greater than for Fe because of the shorter data range of the Mn EXAFS; peak widths are identical when refined for the same k range (k 4–10 Å^{-1}). In addition, the shorter k range and poorer signal to noise ratio for Mn result in the refined Debye-Waller factors for the second and outer shells being much less reliable than those for Fe. Despite the inferior signal to noise ratio for the Mn spectrum, it is clear that significant structural information is present to 5 Å, i.e., a similar range to that found for Fe. The edge position, preedge intensity, first-shell distance, coordination number, and Debye-Waller factor (Table 3) are consistent with the dominant form of Mn

TABLE 3. First-shell EXAFS and near-edge data for staurolite (PF2) and model compounds

	Sample	*N*	*R* (Å)	Cryst. range	$2\sigma^2$ (Å^2)	*E** (eV)	Preedge**
Fe^{2+}	Hedenbergite	6	2.10	(2.07–2.18)†	0.016	8.1	0.020
	(Rb-Fe^{2+})-bearing leucite	4	1.96	1.98‡	0.011	6.4	0.055
Fe^{3+}	Aegirine	6	1.98	(1.94–2.11)	0.021	12.5	0.020
	(K-Fe^{3+})-bearing leucite	4	1.85	1.84‡	0.008	10.1	0.120
	Staurolite	3.6	1.99		0.016	7.8	0.075
Mn^{2+}	Tephroite	6	2.17	(2.14–2.32)	0.023	7.3	0.022
	Willemite	4	2.03	2.05‡	0.010	7.6	0.099
	Staurolite	4.0	2.01		0.012	8.5	0.101
Zn	Smithsonite	6	2.09	(2.11)	0.022		
	Zincite	4	1.96	(1.97–1.99)	0.011		
	Staurolite	5.1	1.95		0.018		
Ti^{4+}	Rutile	6	1.93	(1.94–1.98)	0.019		0.17
	Sphene	(1)	1.74	(1.77)	0.007		0.12
		(5)	1.97	(1.97–2.03)	0.012		
	Ba_2TiO_4	4	1.82	(1.84)	0.006		0.95
	Staurolite	6?	1.86		0.023		0.22

Note: Synthetic XAS model compounds used: $Rb_2FeSi_5O_{12}$ and $KFeSi_2O_6$ with the leucite structure; tephroite; ZnO (Johnson-Matthey); Ba_2TiO_4; all others natural minerals.

* Edge positions relative to metallic Fe (7112 eV) and Mn (6539 eV).

** Intensity of main preedge peak expressed as a fraction of edge step.

† Crystal structure data in parentheses.

‡ Bond length data from Shannon (1976).

being Mn^{2+} in tetrahedral coordination. The Debye-Waller factor for the first Mn-O shell is slightly smaller than that for Fe, again indicating that the Mn environment may be more regular (i.e., with less static disorder) than that of Fe. Alternatively, the smaller Debye-Waller factor may be due to Mn occupying only the tetrahedral site, with some Fe occupying octahedral as well as tetrahedral sites. It is likely that >85% of the Mn_{tot} is in the T2 site.

EXAFS fits and their Fourier transforms for Zn show very similar features to those for Fe and Mn, with similar FT peak widths for the same *k* ranges (Fig. 2). As found for both Fe and Mn, Zn shows that significant structural information is present in the 5-Å region. The refined first-shell distance of 1.96 Å matches that found for $^{[4]}$Zn in ZnO (Table 3), although the refined coordination number and Debye-Waller factors might suggest the presence of both $^{[4]}$Zn and $^{[6]}$Zn. Nevertheless, the refined first-shell bond length and the edge structure provide more reliable information than the coordination and Debye-Waller data, suggesting that the bulk of the Zn (>70%) resides in the T2 sites.

Ti

The expanded absorption edge spectra for Ti in staurolite and model compounds are shown in Figure 3, with preedge and edge data and refined first-shell EXAFS data given in Table 3. Note that the preedge intensity for the model compounds with Fe, Mn, and Ti in tetrahedral coordination increases in the order Fe to Mn to Ti, consistent with the transition probability for the 1s-3d transition being inversely proportional to the population of the 3d site (i.e., 6, 5, and 0 3d electrons, respectively). Greegor et al. (1983) showed that the size of the Ti preedge could be used as a probe for $^{[4]}$Ti. In addition, Waychunas (1987) has shown that the detailed geometry of octahedral sites in different oxide and silicate minerals control the numbers, intensities, and positions of the preedge and edge features.

The spectrum for $^{[4]}$Ti in Ba_2TiO_4 (Fig. 3) is very similar to that shown by Greegor et al. (1983), except that the preedge intensity in our sample is 0.95 (Table 3), compared with 0.85. The spectra for $^{[6]}$Ti in rutile and sphene (titanite) (Fig. 3) are identical to those figured by Greegor et al. (1983) and Waychunas (1987). The latter author has identified up to nine features between 4966 and 5010 eV. The first three are preedge features, the second and third being due to t_{2g} and e_g crystal-field transitions. The fourth occurs on the edge and was assigned to a 1s-4s electronic transition; note that Waychunas and Brown (1990) reassigned this transition in anatase to 1s-4p. The other features are due to multiple scattering and reflect the local geometry of the ligands. Waychunas (1987) showed that the positions of the preedge peaks in oxides and silicates do not vary much with Ti-O bond lengths, although the other main features decrease in energy with increasing Ti-O. He also showed that the preedge intensities are closely related to the degree of distortion of the octahedral site, and he quantified this relationship by relating intensity to bond-angle variance. The energies of the various features in our model compounds were calibrated relative to the first inflection point in metallic Ti and are slightly lower (0.5–1.0 eV) than those reported by Waychunas (1987) for the same minerals. In order to make comparisons between the two data sets, we have arbitrarily added 0.8 eV to our values for staurolite.

The most significant features in staurolite occur at 4968.6, 4982.0, and 4987.5 eV (equivalent to the second, fifth, and sixth features of Waychunas, 1987, respectively). The energy of the preedge peak in staurolite (4968.6 eV) is about 1 eV higher than for $^{[4]}Ti^{4+}$ in Ba_2TiO_4 (4967.5 eV, this work: cf. Waychunas, 1987). It is also about 1 eV higher than that for Ti^{3+} (Waychunas, 1987). These

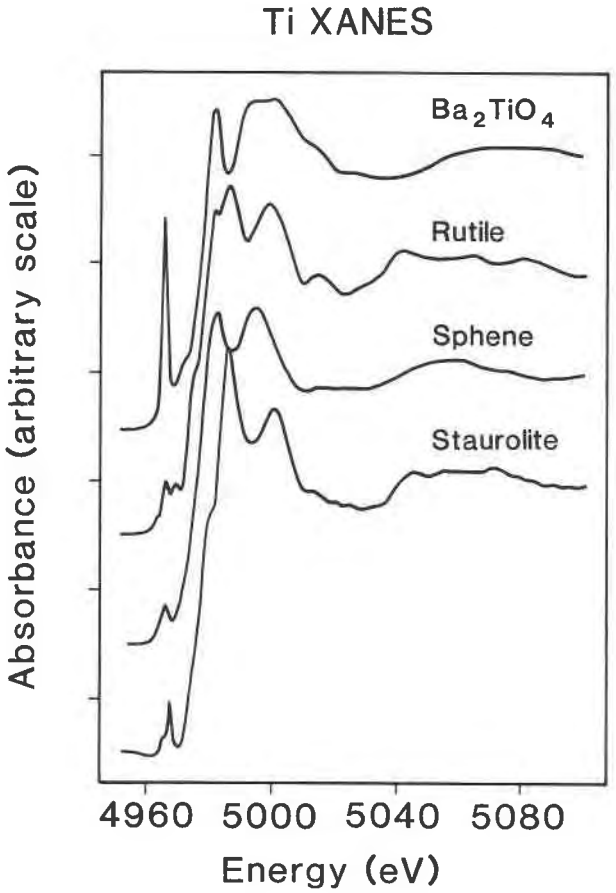

Fig. 3. Expanded background-subtracted Ti K-edge spectra for the edge regions of PF2 staurolite and three model compounds: Ba_2TiO_4 ($^{[4]}$Ti), rutile, and sphene ($^{[6]}$Ti). Note the different preedge intensities and splittings for the different Ti structural environments.

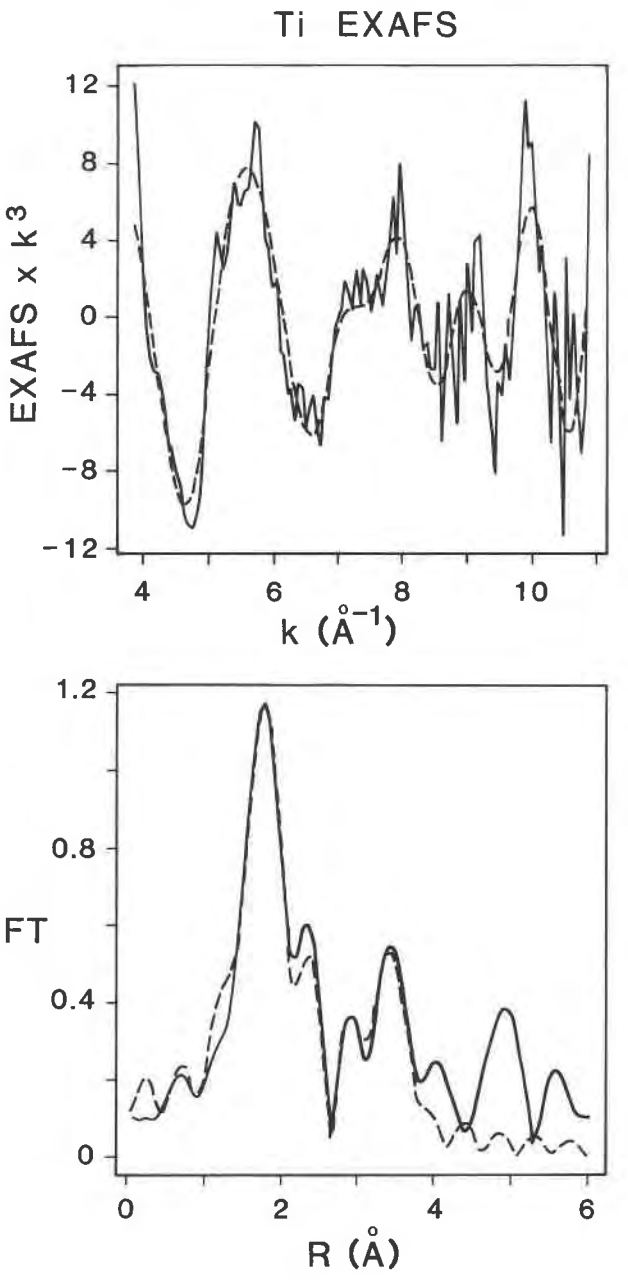

Fig. 4. The k^3-weighted EXAFS ($Å^{-3}$) and Fourier transforms (FT) corrected for phase shifts for Ti in PF2 staurolite. The solid lines represent experimental data and dashed lines calculated fits to the parameters given in Table 4.

differences are believed to be significant, as the precision is better than 1 eV. The intensity of the staurolite preedge peak and the overall appearance of the whole XANES spectrum (Fig. 3, Table 3) are very similar to those for barkevikite and kaersutite (cf. Waychunas, 1987, his Figs. 2, 5). By analogy, it seems probable that Ti in staurolite is present as Ti^{4+} in a distorted octahedral environment. This interpretation is entirely consistent with the assignments of Ti in TiO_2-SiO_2 glasses based on preedge intensities alone (Greegor et al., 1983).

Although the EXAFS spectra are relatively poor and of a limited k-range as a result of the low energy of the K-edge and the low Ti concentration, a refined first shell bond length of 1.86 Å is obtained for a single shell fit, assuming octahedral coordination. This value is similar to the shorter bond lengths for Ti in distorted octahedral environments with O (e.g., rutile and sphene) and is slightly longer than the fourfold distance in Ba_2TiO_4 (Table 3). The refined Debye-Waller factor for staurolite is similar to that for Ti in rutile (Table 3). These data support the assignment of Ti to a distorted octahedrally coordinated environment based on the preedge and edge features alone.

Assuming that Ti is entirely in octahedral sites, the degree of distortion can be deduced from the preedge intensity (Waychunas, 1987) giving a bond-angle variance of about 44 deg^2 for the Ti site in staurolite. This value can be compared with staurolite bond-angle variances for octahedral sites: M1 43–46, M2 44–46, M3 12–17, and M4 86–90 deg^2 (Smyth and Bish, 1988; Bring-

Table 4. Radial information from Ti EXAFS data for staurolite (PF2)

Shell	Ti EXAFS		M2 site crystallography*
	R (Å)	$2\sigma^2$ (Å^2)	R (Å)
6 × O	1.82	0.024	1.905
5 × Al	2.86	0.016	2.858
2 × Fe	2.82	0.007	2.919
3 × Si	3.24	0.002	3.196
2 × Fe	3.32	0.008	3.425

* Radial data calculated for Al in M2 from X-ray crystal structure (Smith, 1968).

hurst and Griffen, 1986). The dominant elements occupying these sites are Al in M1–M3 and Fe^{2+} in M4 (Hawthorne et al., 1993). Hawthorne (1978) has shown that the octahedral cation sites in clinoamphiboles show the same relative distortions (M3 > M1 > M2) irrespective of which elements occupy the sites. Thus, assuming that the main control of site distortion is overall structure, we suggest that Ti in Pizzo Forno staurolite is located in either M1 or M2, i.e., in the kyanite-like layer.

Ward (1984) suggested that the color in staurolite is due to Fe^{2+}-Ti^{4+} charge transfer in adjacent T2 sites, whereas Ståhl et al. (1988) concluded that electron transfer occurred between Fe in T2 site and Ti in either M2 or M3 sites. The XAS site distortion data suggest that the M2 site is more likely. We have tested this further by fitting outer shell data to the EXAFS Ti spectrum using shells of atoms modeled on Al in each of the M1–M3 octahedral sites. The fit obtained for Ti in M2 was by far the best, with the M1 and M3 models showing very poor fits to the Fourier transform peaks in the range 3–4 Å. Figure 4 shows the fit for M2 out to 3.3 Å; data quality does not justify fitting more distant shells. The calculated EXAFS data are given in Table 4 and compared with X-ray crystal structure data. Note that the agreement is good, bearing in mind that the EXAFS results are specific to Ti, whereas the X-ray data are for Al, which is the dominant element in this site. We conclude that the Ti EXAFS can be closely simulated using a model that matches the pattern of the shells around the M2 site, supporting the above deductions.

Concluding remarks

1. Our principal conclusions regarding the site assignments of Fe, Mn, Zn, and Ti are summarized in Table 1, where they can be compared with the recommendations of other workers. The best agreement is with the predictions of Holdaway et al. (1991), but note that our work confirms their second choice for the siting of Ti, i.e., in M2.

2. The chemical and structural complexities of staurolite have combined to present researchers with problems, many of which seemed intractable. Making site assignments for both major and minor elements seemed to be an exercise in deductive reasoning based on insufficient evidence. With the current availability of new methods for structural analysis, staurolite is slowly yielding up some of its secrets. The present study points to the valuable role of the element-specific XAS technique in structural studies of chemically complex solid solutions.

Acknowledgments

We thank the Natural Environment Research Council for the award of research grant GR3/6653, M.J. Holdaway for providing the sample of staurolite (PF2, Pizzo Forno, Switzerland), and Frank Hawthorne for providing a copy of his magnum opus on staurolite structure. Simon Kohn and Gordon Cressey contributed to useful discussions and provided critical comments on an early version of this paper, and Michael Holdaway, Barbara Dutrow, and Peggy O'Day provided detailed and perceptive reviews.

References cited

Alexander, V.D. (1989) Iron distribution in staurolite at room and low temperatures. American Mineralogist, 74, 610–619.

Ashworth, J.R. (1975) Staurolite at anomalously high grade. Contributions to Mineralogy and Petrology, 53, 281–291.

Binsted, N., Greaves, G.N., and Henderson, C.M.B. (1986) Fe K-edge absorption spectroscopy of silicate minerals and glasses. Journal de Physique, Colloque C8, 47, 837–840.

Binsted, N., Gurman, S.J., and Campbell, J.W. (1988) SERC Daresbury Laboratory EXCURVE88 program. Daresbury, U.K.

Bringhurst, K.N., and Griffen, D.T. (1986) Staurolite-lusakite series. II. Crystal structure and optical properties of a cobaltoan staurolite. American Mineralogist, 71, 1466–1472.

Brown, G.E., Calas, G., Waychunas, G.A., and Petiau, J. (1988) X-ray absorption spectroscopy: Applications in mineralogy and geochemistry. In Mineralogical Society of America Reviews in Mineralogy, 18, 431–512.

Calas, G., and Petiau, J. (1982) Short-range order around Fe(II) and Mn(II) in oxide glasses determined by X-ray absorption spectroscopy in relation with other spectroscopic and magnetic properties. In P.H. Gaskell, E.A. Davis, and J.M. Parker, Eds., Structure of non-crystalline materials II, p. 18–28. Taylor and Francis, London.

——— (1983) Coordination of iron in oxide glasses through high-resolution K-edge spectra: Information from the pre-edge. Solid State Communications, 48, 625–629.

Dutrow, B.L., Holdaway, M.J., and Hinton, R.W. (1986) Lithium in staurolite and its petrologic significance. Contributions to Mineralogy and Petrology, 94, 496–506.

Dyar, M.D., Perry, C.L., Rebbert, C.R., Dutrow, B.L., Holdaway, M.J., and Lang, H.M. (1991) Mössbauer spectroscopy of synthetic and naturally occurring staurolite. American Mineralogist, 76, 27–41.

Ganguly, J. (1968) Analysis of the stabilities of chloritoid and staurolite and some equilibria in the system FeO-Al_2O_3-SiO_2-H_2O-O_2. American Journal of Science, 266, 277–298.

Greegor, R.B., Lytle, F.W., Sandstrom, D.R., Wong, J., and Schultz, P. (1983) Investigation of TiO_2-GeO_2 glasses by X-ray absorption spectroscopy. Journal of Non-Crystalline Solids, 55, 27–43.

Guidotti, C.V. (1970) The mineralogy and petrology of the transition from the lower to upper sillimanite zone in the Oquossoc Area, Maine. Journal of Petrology, 11, 277–336.

Gurman, S.J., Binsted, N., and Ross, I. (1984) A rapid exact curved-wave theory for EXAFS calculations. Journal of Physics C: Solid State Physics, 17, 143–151.

Hawthorne, F.C. (1978) The crystal chemistry of the amphiboles. VI. The stereochemistry of the octahedral strip. Canadian Mineralogist, 16, 37–52.

Hawthorne, F.C., Ungaretti, L., Oberti, R., Caucia, F., and Callegari, A. (1993) The crystal chemistry of staurolite. I. Crystal structure and site occupancies. Canadian Mineralogist, in press.

Holdaway, M.J., Dutrow, B.L., and Shore, P. (1986) A model for the crystal chemistry of staurolite. American Mineralogist, 71, 1142–1159.

Holdaway, M.J., Mukhopadhyay, B., Dyar, M.D., Dutrow, B.L., Rumble, D., and Grambling, J.A. (1991) A new perspective on staurolite crystal

chemistry: Use of stoichiometric and chemical end-members for a mole fraction model. American Mineralogist, 76, 1910–1919.

Joyner, R.W., Martin, K.J., and Meehan, P. (1987) Some applications of statistical tests in analysis of EXAFS and SEXAFS data. Journal of Physics C: Solid State Physics, 20, 4005–4012.

Lee, P.A., and Pendry, J.B. (1975) Theory of extended X-ray absorption fine structure. Physics Reviews, B11, 2795–2811.

Náray-Szabó, I., and Sasvári, K. (1958) On the structure of staurolite, $HFe_2Al_9Si_4O_{24}$. Acta Crystallographica, 11, 862–865.

Ribbe, P.H. (1982) Staurolite. In Mineralogical Society of America Reviews in Mineralogy, 5, 171–187.

Shannon, R.D. (1976) Revised effective ionic radii and systematic studies of interatomic distances in halides and chalcogenides. Acta Crystallographica, A32, 751–767.

Smith, J.V. (1968) The crystal structure of staurolite. American Mineralogist, 53, 1139–1155.

Smyth, J.R., and Bish, D.L. (1988) Crystal structures and cation sites of the rock-forming minerals, 332 p. Allen and Unwin (Unwin-Hyman), Boston.

Ståhl, K., and Legros, J.-P. (1991) On the crystal structure of staurolite: The X-ray crystal structure of staurolite from the Pyrenees and Brittany. Acta Crystallographica, B46, 292–301.

Ståhl, K., Kvick, Å., and Smith, J.V. (1988) A neutron diffraction study of hydrogen positions at 13K, domain model, and chemical composition of staurolite. Journal of Solid State Chemistry, 73, 362–380.

Tagai, T., and Joswig, W. (1985) Untersuchungen der Kationenverteilung im Staurolith durch Neutronenbeugung bei 100K. Neues Jahrbuch für Mineralogie Monatshefte, 97–107.

Takéuchi, Y., Aikawa, N., and Yamamoto, T. (1972) The hydrogen locations and chemical composition of staurolite. Zeitschrift für Kristallographie, 136, 1–22.

Ward, C.M. (1984) Titanium and the color of staurolite. American Mineralogist, 69, 541–545.

Waychunas, G.A. (1987) Synchrotron radiation XANES spectroscopy of Ti in minerals: Effects of Ti bonding distances, Ti valence, and site geometry on absorption edge structure. American Mineralogist, 72, 89–101.

Waychunas, G.A., and Brown, G.E. (1990) Polarized X-ray absorption spectroscopy of metal ions. Physics and Chemistry of Minerals, 17, 420–430.

Waychunas, G.A., Apted, M.J., and Brown, G.E. (1983) X-ray K-edge absorption spectra of Fe minerals and model compounds: Near-edge structure. Physics and Chemistry of Minerals, 10, 1–9.

Yardley, B.W.D. (1981) A note on the composition and stability of Fe-staurolite. Neues Jahrbuch für Mineralogie Monatshefte, 127–132.

Manuscript received January 24, 1992
Manuscript accepted December 28, 1992